

This is the peer reviewed version of the following article: Ai, Z. T., & Mak, C. M. (2016). Large eddy simulation of wind-induced interunit dispersion around multistory buildings. *Indoor Air*, 26(2), 259-273, which has been published in final form at <https://doi.org/10.1111/ina.12200>. This article may be used for non-commercial purposes in accordance with Wiley Terms and Conditions for Use of Self-Archived Versions. This article may not be enhanced, enriched or otherwise transformed into a derivative work, without express permission from Wiley or by statutory rights under applicable legislation. Copyright notices must not be removed, obscured or modified.

Large eddy simulation of wind-induced interunit dispersion around multistory buildings

Short title: LES investigation of interunit dispersion

Z.T. Ai

Department of Building Services Engineering, The Hong Kong Polytechnic University, Hong Kong

E-Mail: zhengtao.ai@connect.polyu.hk

C.M. Mak (Corresponding author)

Department of Building Services Engineering, The Hong Kong Polytechnic University, Hong Kong

Tel.: +852 2766 5856; Fax: +852 2765 7198

E-Mail: cheuk-ming.mak@polyu.edu.hk

Abstract: Previous studies regarding interunit dispersion used Reynolds-averaged Navier-Stokes (RANS) models and thus obtained only mean dispersion routes and re-entry ratios. Given that the envelope flow around a building is highly fluctuating, mean values could be insufficient to describe interunit dispersion. This study investigates the wind-induced interunit dispersion around multistory buildings using the large eddy simulation (LES) method. This is the first time interunit dispersion has been investigated transiently using a LES model. The quality of the selected LES model is seriously assured through both experimental validation and sensitivity analyses. Two aspects are paid special attention: (a) comparison of dispersion routes with those provided by previous RANS simulations and (b) comparison of time scales with those of natural ventilation and the survival times of pathogens. The LES results reveal larger dispersion scopes than the RANS results. Such larger scopes could be caused by the fluctuating and stochastic nature of envelope flows, which, however, is cancelled out by the inherent Reynolds-averaged treatment of RANS models. The time scales of interunit dispersion are comparable with those of natural ventilation. They are much shorter than the survival time of most pathogens under ordinary physical environments, indicating that interunit dispersion is a valid route for disease transmission.

Keywords: Interunit dispersion, airborne infection, time scales, multistory buildings, large eddy simulation (LES), computational fluid dynamics (CFD)

Practical implications: The transient characteristics of interunit dispersion revealed by LES

simulations have significantly increased our current understanding of this type of dispersion. This improved knowledge regarding dispersion mechanisms, dispersion routes, and time scales can contribute to improved control measures for airborne infectious diseases. The modeling and numerical methods described in this study are useful for future studies of pollutant dispersion around built environments.

1. Introduction

Many epidemiological and engineering studies have shown that airborne transmission is a major person-to-person respiratory transmission route (e.g., Barker et al., 2001; Mendell et al., 2002; Cole and Cook, 1998; Nicas et al., 2005; Tellier, 2006; Hodgson et al., 2012; Morawska et al., 2013). As a special airborne transmission route, interunit dispersion, namely cross transmission between units in the same building, was identified in Hong Kong during the outbreak of SARS in 2003 (HWFB-HK, 2003, Yu et al., 2004). Apart from dispersion through interior doors and window leakage (Yu et al., 2004; Li et al., 2005a, b), dispersion through open windows in building envelopes has attracted increasing attention (Niu and Tung, 2008; Gao et al., 2008, 2009; Wang et al., 2010; Liu et al., 2010, 2011a, b; Ai et al., 2013a; Ai and Mak, 2014a). The present study only focuses on the latter, which usually exists in residential buildings where natural ventilation through open windows is the most common ventilation mode. Such interunit dispersion can be a valid route for disease transmission, essentially because of the short dispersion distances between units in the same building and the large openings that may involve considerable airflow exchanges.

The results of on-site measurements (Niu and Tung, 2008) and CFD simulations (Gao et al.,

2008) on buoyancy-dominated interunit dispersion provided sound explanation of the upward transmission of SARS in the Amoy Gardens housing complex (HWFB-HK, 2003). Later, a series of wind tunnel experiments (Wang et al., 2010; Liu et al., 2010, 2011a, b) revealed that wind-induced interunit dispersion could occur along both horizontal and vertical directions. However, it was difficult to take accurate measurements of the indoor concentration level in a wind tunnel experiment using highly reduced-scale models (Mfula et al., 2005). Considering the uncontrollable boundary conditions of an on-site measurement and the scale problem of wind tunnel experiments (van Hooff and Blocken, 2010), Ai et al. (2013a) and Ai and Mak (2014a) used CFD methods to study the wind-dominated interunit dispersion around multistory buildings. Their CFD results identified typical interunit dispersion routes and quantified re-entry ratios, demonstrating the severity of interunit dispersion. Their studies also suggest that the CFD method is a suitable research tool for the study of interunit dispersion. However, they used RANS models and thus only obtained mean dispersion routes and re-entry ratios. Considering the highly fluctuating characteristics of a coupled indoor and outdoor flow (Haghighat et al., 1991, 2000; Linden, 1999; Straw, 2000; Etheridge, 2011; Ai and Mak, 2014c), the mean results may not be sufficient to describe an interunit dispersion process. In addition, the time scales of interunit dispersion, which cannot be obtained from a steady simulation, are important for an infectious risk assessment. Therefore, a transient investigation of interunit dispersion using an advanced numerical model, such as LES, is necessary.

The present study intends to provide such an investigation using an LES model. LES models are recognized as advanced models, as they directly and transiently resolve those

large-scale eddies that make a dominant contribution in transporting momentum, mass, and energy (Fluent, 2010). Many studies comparing the performance of RANS and LES models (e.g., Murakami, 1993; Rodi, 1997; Jiang and Chen, 2001; Tominaga and Stathopoulos, 2010, 2011; Gousseau et al., 2011a; Salim et al., 2011; Caciolo et al., 2012) have clearly demonstrated the superiority of LES models in predicting both flow and concentration fields in built environments, although LES modeling requires greater computational resources.

Pathogen-laden aerosols are simulated using passive tracer gas, which has been widely used in previous studies of pollutant dispersion (Riley et al., 1978; Gao et al., 2008; Niu and Tung, 2008; Wang et al., 2010; Liu et al., 2010, 2011a, b; Ai et al., 2013a; Ai and Mak, 2014a). The rationality of using tracer gas is also supported by some studies regarding the size and behavior of respiratory droplet-nuclei (Wells, 1934; Mitman, 1945; Duguid, 1946; Brundrett, 1992; CDCP, 1994; Nicas et al., 2005; Morawska, 2006; Tellier, 2006; Gao et al., 2009). In particular, Duguid (1946) showed that respiratory droplet-nuclei are most commonly between 1 and 2 μm in diameter. A review by Morawska (2006) showed that viruses range from 0.02 to 0.3 μm in diameter; for instance, an individual SARS coronavirus ranges from 0.075 to 0.16 μm and an influenza virus is of a similar size. Simulations by Gao and colleagues (2007, 2009) suggested that aerosols with diameters less than 2.5 μm disperse like gaseous pollutants. The smaller aerosols are less influenced by gravity than larger aerosols, which thus could suspend in air for a longer time and be transported over a greater distance by airflows (Xie et al., 2007; Morawska et al., 2013). In addition, these smaller aerosols have a chance to deposit in the lower respiratory tract and thus could cause serious negative effects on human health (Tellier, 2006, Thomas, 2013). Despite of the need to investigate smaller aerosols, the

importance of larger aerosols in disease transmission (Thomas, 2013) should not be ignored, which, however, cannot be represented by tracer gas.

By analyzing the transient evolution of tracer gas concentration in a source unit and its adjacent units, one can estimate dispersion routes, re-entry possibilities, and dispersion time scales. Special attention is paid to two aspects: (a) comparison of the transient dispersion characteristics with the mean values obtained previously using RANS models (Ai et al., 2013a; Ai and Mak, 2014a) and (b) comparison of the dispersion time scales with those of airflow replacement of natural ventilation and the survival times of viruses.

2. CFD method: case setup

This section describes the detailed numerical method as well as the approach used to evaluate interunit dispersion. Reasons for selecting the present CFD method are also discussed.

2.1. Numerical simulation of flow and dispersion

By filtering the time-dependent Navier-Stokes equations, the governing equations used for large eddies of an incompressible flow of a Newtonian fluid can be obtained:

$$\frac{\partial \bar{u}_i}{\partial x_i} = 0 \quad (1)$$

$$\frac{\partial (\rho \bar{u}_i)}{\partial t} + \frac{\partial (\rho \bar{u}_i \bar{u}_j)}{\partial x_j} = \frac{\partial \sigma_{ij}}{\partial x_j} - \frac{\partial \bar{p}}{\partial x_i} - \frac{\partial \tau_{ij}}{\partial x_j} \quad (2)$$

where the overbars denote the filtered variables, the term σ_{ij} is the stress tensor because of molecular viscosity (μ), and the additional term τ_{ij} is the subgrid-scale stress term defined as $\tau_{ij} \equiv \overline{\rho u_i u_j} - \overline{\rho} \bar{u}_i \bar{u}_j$. This term represents the impact of non-resolved small-scale eddies on large-scale eddies. As τ_{ij} in the LES model is unknown, modeling is needed to close the

governing equations. The Boussinesq hypothesis (Hinze, 1975) is used to correlate τ_{ij} with the strain rate tensor $\overline{S_{ij}}$ through the following expression:

$$3\tau_{ij} - \tau_{kk}\delta_{ij} = -6\mu_{SGS}\overline{S_{ij}} \quad (3)$$

Here the isotropic part τ_{kk} is zero for an incompressible flow. In this study, the subgrid-scale turbulent viscosity μ_{SGS} is modeled by the Smagorinsky-Lilly model (Smagorinsky, 1963; Lilly, 1992). In this model, μ_{SGS} is calculated by:

$$\mu_{SGS} = (C_s\Delta)^2 \sqrt{2\overline{S_{ij}}\overline{S_{ij}}} \quad (4)$$

where the Smagorinsky constant C_s is empirically given as 0.1 and Δ is the grid scale. This model and the constant 0.1 have been most frequently used in the study of urban and building aerodynamics (e.g., Tominaga and Stathopoulos, 2010; Ai and Mak, 2014b, c). Although the dynamic Smagorinsky-Lilly model can obviate specifying a constant C_s , it shows some computational instability and a small deficiency in predicting near-wall flows (Iizuka and Kondo, 2004; Ai and Mak, 2014d).

The concentration field of the tracer gas is simulated by solving a concentration equation, written as:

$$\frac{\partial(\overline{c_i})}{\partial t} + \frac{\partial(\overline{c_i u_j})}{\partial x_j} = \frac{\partial}{\partial x_j} \left[\left(\frac{\mu}{Sc} + \frac{\mu_{SGS}}{Sc_{SGS}} \right) \cdot \frac{\partial \overline{c_i}}{\partial x_j} \right] + \overline{S_i} \quad (5)$$

where c_i represents the concentration of tracer gas (ppm), μ is the dynamic viscosity coefficient (m²/s), Sc is the Schmidt number (equal to 1.0), Sc_{SGS} is the turbulent Schmidt number for SGS motions (specified as 0.4), and S_i is the generation rate of source (ppm/s).

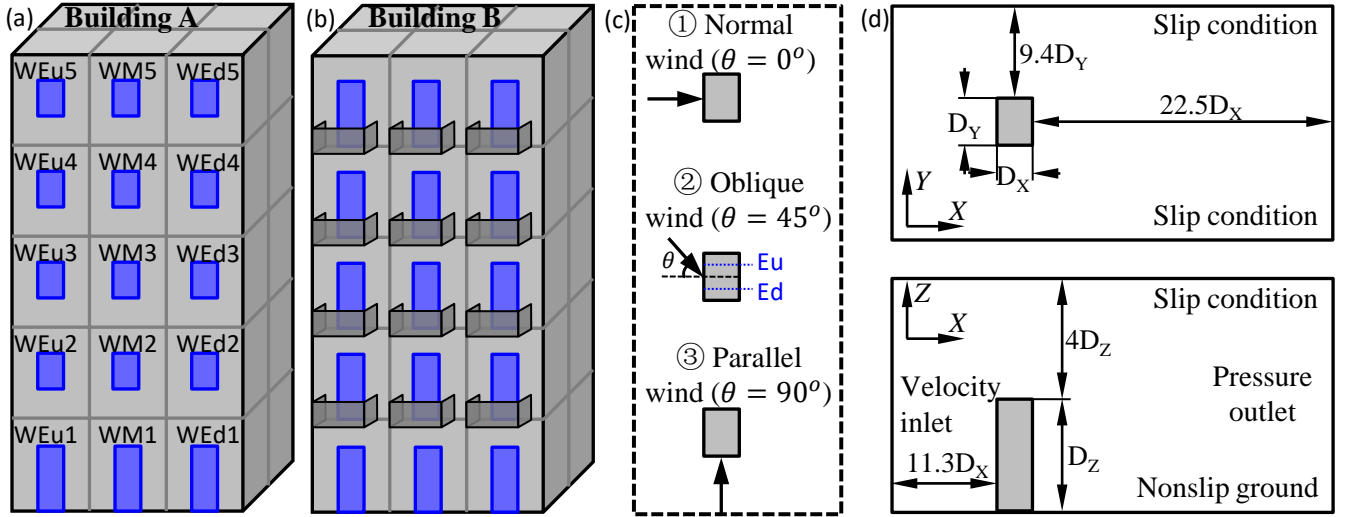


Fig. 1 Hypothetical building models (a)-(b), wind directions (c), and computational domain (d),

where (d) provides only a schematic view of the layout of the buildings and the domain.

2.2. Model geometry, computational domain, and grid

A five-story generic building (Building A in Fig. 1 (a)) with six units on each floor is constructed to investigate the transient interunit dispersion of pollutants via open windows on external facades of multistory buildings. This building model is selected as a compromise between numerical cost and the expectation of examining upward, downward, and lateral dispersions. The room dimensions are $3.1\text{m} (X) \times 2.4\text{m} (Y) \times 2.7\text{m} (Z)$, while the opening dimensions are $0.75\text{m} (Y) \times 1.2\text{m} (Z)$ on the upper four floors and $0.7\text{m} (Y) \times 2.0\text{m} (Z)$ on the first floor. The height of the windowsills on the upper four floors is 0.8m . These dimensions are modeled exactly on those measured in a real building in Hong Kong (Niu and Tung, 2008).

This generic building is simulated as a 1:30 reduced-scale model, considering that a small model is convenient for creating a sufficiently fine mesh for LES, which normally requires a near-wall y^+ to be close to unity or at least less than 5 (Fluent, 2010). This reduced-scale model fulfills similarity requirements (see Ai et al., 2013a). To study the influence of an

envelope feature on interunit dispersion, Building B (see Fig. 1 (b)) is constructed with balconies (Building Department, Lands Department and Planning Department, 2001). The dimensions of the balconies are $0.9\text{m} (X) \times 1.8\text{m} (Y) \times 0.9\text{m} (Z)$. The opening dimensions for all rooms in Building B are $0.75\text{m} (Y) \times 2.0\text{m} (Z)$.

Table 1 A summary of the cases investigated in the present study; note that two building types, with and without balconies, are considered for each case.

Case	$\theta = 0^\circ$ & windward side	$\theta = 0^\circ$ & leeward side	$\theta = 45^\circ$ & windward side	$\theta = 45^\circ$ & leeward side	$\theta = 90^\circ$ & lateral side
Source unit	WM3	LM2	WEu3	LM2	Ed2

Three prevailing wind directions, namely, normal (0°), oblique (45°), and parallel (90°), are considered (see Fig. 1 (c)). The units are named as partly shown in Fig. 1 (a), where W indicates the windward side, L the leeward side, Eu the upstream-end units, M the middle units, Ed the downstream-end units, and numbers one to five the stories. The present study investigates ten cases, as listed in Table 1. These cases are selected as they represent different dispersion patterns around a façade under a specific wind direction (see Ai and Mak, 2014a).

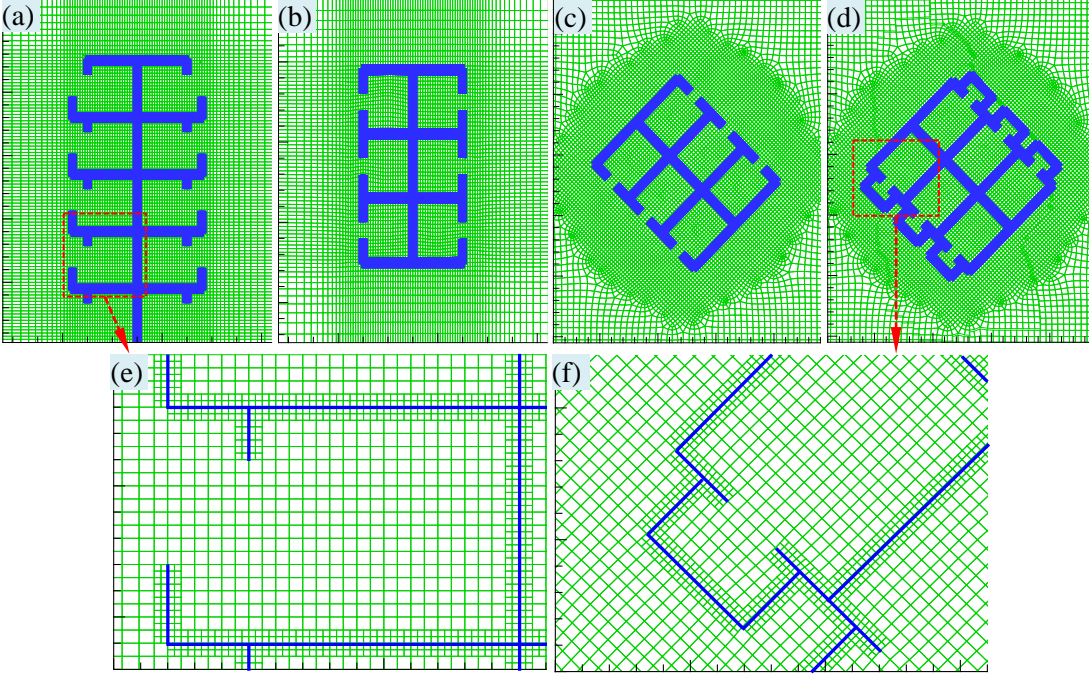


Fig. 2 Mesh information: (a) $\theta = 0^\circ$ side view with balconies, (b) $\theta = 0^\circ$ plan view without balconies, (c) $\theta = 45^\circ$ plan view without balconies, (d) $\theta = 45^\circ$ plan view with balconies, and (e)-(f) detailed local mesh information; the thick lines in (a)-(d) contain not only the walls between units but also very fine near-wall meshes showing in (e)-(f).

The two hypothetical buildings are separately placed in a computational domain, as shown in Fig. 1 (d). The domain dimensions are selected following the best practice guidelines (e.g., Franke et al., 2007; Yoshie et al., 2007; Tominaga et al., 2008), resulting in a maximum blockage ratio of 1.01%. The body-fitted mesh-generation technique suggested by van Hooff and Blocken (2010) is adopted to take full control of mesh quality, particularly in the region immediately close to the building. Near the domain ground and the building surfaces, we use a local refining method (Ai and Mak, 2014b) that doubles the mesh number of the first cells both horizontally and vertically in a hemisphere zone. Finally, the computational domain is constructed from around 6.0×10^6 hexahedral cells with a minimum cell width of $5 \times 10^{-5} \text{m}$ (around $1 \times 10^{-4} H_b$) and a maximum stretching ratio of 1.16 (compared to 1.18 in Ai and Mak,

2014a). Such a small minimum cell width, in combination with $U_H=2\text{m/s}$, results in an average y^+ value of around 2.0 for the domain ground and the building surfaces (1.0 near the building), U_H is the reference wind speed at the height of building. A schematic view of mesh information in and around the buildings is given in Fig. 2. The sensitivity analysis of the mesh resolution is described in Section 3.

2.3. Boundary conditions

The inlet boundary conditions of the computational domain are defined using the profiles of the mean wind speed U , turbulent kinetic energy k , and turbulent dissipation rate ε , as indicated by Eqs. (6), (7), and (8), respectively:

$$U = \frac{u^*}{\kappa} \ln \left(\frac{z + z_0}{z_0} \right) \quad (6)$$

$$k = \sqrt{M_1 \cdot \ln(z + z_0) + M_2} \quad (7)$$

$$\varepsilon = \frac{u^* \sqrt{C_\mu}}{\kappa(z + z_0)} \sqrt{M_1 \cdot \ln(z + z_0) + M_2} \quad (8)$$

The aerodynamic roughness height ($z_0 = 0.75 \text{ mm}$) is selected based on the roughness condition in an average wind tunnel (Leitl and Schatzmann, 1998). Based on the reference wind speed $U = 2 \text{ m/s}$ at the building height of $z = 0.45 \text{ m}$ and the von Karman constant $\kappa = 0.4187$, a logarithmic mean wind speed profile (Eq. (6)) can be obtained, with the friction velocity $u^* = 0.13 \text{ m/s}$. The model coefficients M_1 and M_2 in the turbulence profiles are obtained from fitting the measured k profile in the wind tunnel of Leitl and Schatzmann (1998); they equal 0.025 and 0.41, respectively. The empirical constant C_μ is specified as 0.001 (Ai and Mak, 2014a). Based on the predefined k and ε profiles, the fluctuation in the mean velocity profile at the inlet plane is generated using the Vortex method (Mathey et

al., 2006) with 190 vortices. Zero static pressure (that is, zero normal gradients of all variables) is adopted on the domain outlet, while the zero normal velocity and the zero normal gradients of all variables are used on the top and lateral sides (Ai and Mak, 2013b). The building surfaces and the domain ground are simply defined as a condition having nonslip walls shear stress, as no existing formula for the LES model takes into account the roughness of walls. Although roughness could be modelled explicitly using roughness elements, it would increase the numerical cost significantly. Some previous studies (Gousseau et al., 2011a; Tominaga and Stathopoulos, 2011; Ai and Mak, 2014b, c) show that using this non-slip wall condition can lead to reasonable results. With regard to dispersion simulation, the tracer gas CO₂ is released in the center of a source unit and the evolution of concentrations in all units is then examined to record its dispersion characteristics. The CO₂ is generated constantly at a rate of 8.0mg/s. This emission rate is low enough to avoid the density effect on the dispersion and on the calculation of ventilation rate.

2.4. Other computational parameters

The widely used commercial CFD code Fluent 13.0.0 (Fluent, 2010), incorporating a series of user-defined functions (UDF), is used to conduct the numerical modeling. The LES model is used to predict both flow and concentration fields transiently. The governing equations are discretized to algebraic equations based on the finite volume method (FVM). The discretization method for the pressure and diffusive terms is a second-order scheme, whereas a second-order bounded central-differencing scheme is used for the convective term. A second-order implicit scheme is used for temporal discretization. Finally, the pressure-velocity coupling method is SIMPLEC. The convergence of each time step is achieved when both the

area averaged wind speed and CO₂ concentration at the opening of the source unit are stable for at least five iterations. Based on the converged mean flow and concentration fields generated by a RANS model, the transient simulation of flow and concentration fields using the LES model continues for a sufficient period of time (approximately 3 flow-through time T_{ft} , namely $1200 \Delta t^*$ in the present study) to avoid the influence of initial conditions and to obtain statistically stable average results, where $T_{ft} = D_L / U_H$ with D_L the domain length, and Δt^* is the nondimensional time step size, defined as $\Delta t^* = \Delta t \times U_H / H$ with Δt the time step size. Here Δt^* is equal to 0.044. Note that at this stage the concentration field corresponds to a background tracer gas, which is O₂ in the present study. Then the tracer gas CO₂ is generated in the source unit, and the transient flow and concentration fields are computed simultaneously. It is found that pre-charging a background tracer gas can effectively avoid the unexpected solution oscillation caused by a sudden introduction of the concentration equation (see an example in Fig. 3). Both the ACH (air change per hour, h⁻¹) values of units and the average concentration at respiration planes for standing position (at the height of 1.6m from the floor) are then continuously recorded.

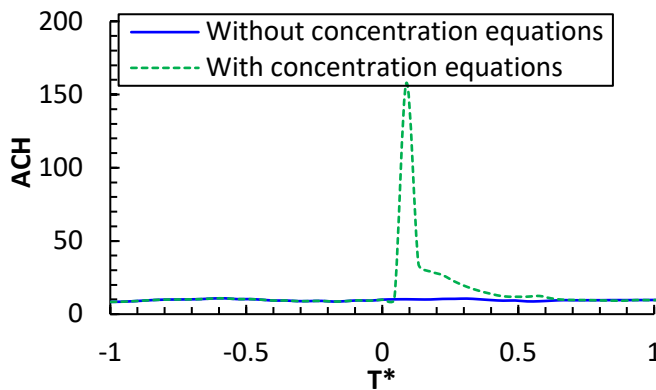


Fig. 3 Effect of introducing the concentration equation to the prediction of ACH value for unit WM3; the concentration equation is introduced at $T^*=0$, where T^* is the nondimensional time,

$$T^* = T \times U_H / H .$$

2.5. Interunit dispersion evaluation

Besides the concentration ratio, this study uses a composite parameter ‘re-entry ratio’ proposed by Niu and Tung (2008) to evaluate the interunit dispersion. The re-entry ratio, R_k , is defined as the fraction of the exhaust air from a source unit i that re-enters another unit j .

It can be calculated by the following equation:

$$R_k = M_{i-j} \frac{V_j (ACH)_j}{V_i (ACH)_i} \quad (9)$$

where the concentrations ratio, M_{i-j} , is defined as the pollutant concentration of air that originates from the source unit i and is present in another unit j ; V_i and V_j are unit volumes, which are the same in the present study. An instantaneous M_{i-j} can be calculated from the predicted instantaneous mean concentrations in two units, $M_{i-j} = C_j / C_i$. Here, the concentration in a unit (C_i or C_j) is represented by the spatial mean concentration on the aforementioned respiration plane.

The ACH value of a unit is calculated using the integration method, integrating velocities throughout an opening (Jiang and Chen, 2001; Ai and Mak, 2014b). An instantaneous ventilation rate is obtained by integrating the velocities from an instantaneous flow field:

$$ACH = \frac{\sum_{m=1}^M \sum_{n=1}^N |U_{m,n}| \Delta y_m \Delta z_n}{2V} \quad (10)$$

where $U_{m,n}$ is the normal-to-opening velocity component at the opening area of $\Delta y_m \times \Delta z_n$, and V is the unit volume. The ACH values calculated by the integration method correspond only to the mean flow induced ventilation rates, which means only advective flow exchange is included. **The ACH values are calculated based on the model scale used in the present study.**

3. CFD simulation: Validation and sensitivity test

This section describes the CFD validation and detailed sensitivity analyses of some important computational parameters that may influence the reliability of the numerical results.

3.1. Experimental validation

The interunit dispersion in multistory buildings investigated in the present study involves two elementary flow and dispersion problems: (a) coupled indoor and outdoor airflow, specifically single-sided natural ventilation, and (b) gaseous dispersion in and around a naturally ventilated building. A previous experiment by Dascalaki et al. (1996), which includes the two elementary problems, validated the numerical method described in Section 2. A detailed comparison between the simulated results and the measured data can be found in our previous papers (Ai and Mak, 2014b, c). The predicted ACH value (it is 12.89h^{-1}) shows a very good agreement with the measured data (it is $9.60\text{-}13.18\text{h}^{-1}$). This comparison justifies the use of the LES model and concentration method in the prediction of flow and dispersion in naturally ventilated buildings. The general computational settings in the present study are the same with those in the previous papers (Ai and Mak, 2014b, c).

3.2. Influence of spatial resolution

The mesh quality is assured in three aspects. First, the mesh is arranged based on our previous mesh sensitivity test (against experimental data) on a similar flow problem (Ai and Mak, 2014b, c). Second, the mesh resolution, especially in regions on and close to building surfaces, strictly follows the best practice guidelines, such as the COST (Franke et al., 2007) and AIJ (Tominaga, 2008). Third, for each wind direction, two grids with different resolutions (y^+ around 2.0 and 4.0) are created, and then the Grid Convergence Index (GCI) (Roache,

1994) based on the Richardson extrapolation method (Richardson, 1910) is calculated to show the relative errors of the grids. The ACH values of the 30 units in the multistory buildings are used to represent numerical solutions. The values of the finer mesh based $GCI_{(ACH)}$ are all below 3.0%, indicating that the finer grid (with y^+ around 2.0) is generally grid converged.

3.3. Influence of temporal resolution

Besides 0.044, two other time step sizes (indicated by Δt^*), namely 0.022 and 0.22, are also tested. We compare the power spectra in the frequency domain for ACH values generated using the three time step sizes. Fig. 4 presents the comparison for unit WM3 under normal wind direction. Generally, the two smaller time steps, 0.044 and 0.022, predict very close dominant frequencies with similar amplitudes, which deviate significantly from those given by 0.22. This comparison demonstrates that the time step 0.044 is small enough to cover the high frequencies that have pronounced influence on interunit dispersion (Franke et al., 2007), and thus further reduction down to 0.022 is unnecessary, while 0.22 is too large to realize the effect of those important high-frequency flows.

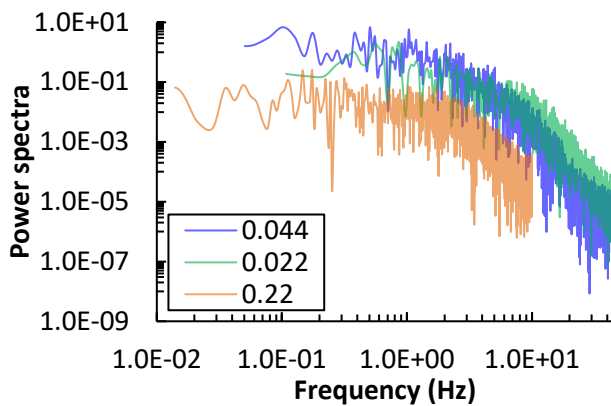


Fig. 4 Power spectra in the frequency domain for the ACH value of unit WM3 under normal wind direction; the legend indicates the nondimensional time step sizes.

3.4. Influence of inflow conditions

The turbulent characteristics of inflow conditions are always an important issue of concern for LES modeling. Tabor and Baba-Ahmadi (2010) systematically reviewed the generating methods of the inflow condition for LES, suggesting that each method has its advantages and disadvantages. Recently, studies by Ai and Mak (2014b) indicated that there is no universal inflow generating method and the optimum method should be flow problem dependent. Later, Ai and Mak (2014d) compared the fluctuating characteristics of the nondimensional velocity components ($u^* = u/U_H$, $v^* = v/U_H$, $w^* = w/U_H$) that are produced by several inflow generating methods, demonstrating that a specific type of generating method represents a specific type of inflow condition. In the present study, the Vortex Method (Fluent, 2010) is selected to consider a highly fluctuating inflow condition.

4. Results and analyses: General flow and dispersion characteristics

This section intends to provide background flow and dispersion information for the later analyses of interunit dispersion routes and time scales.

Table 2 Comparison of reattachment lengths on the roof and on downstream ground.

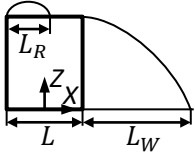
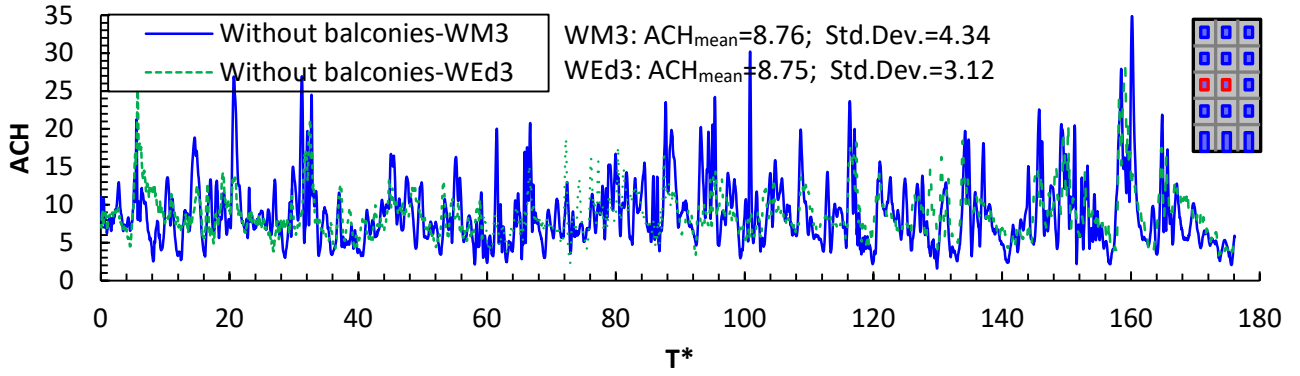
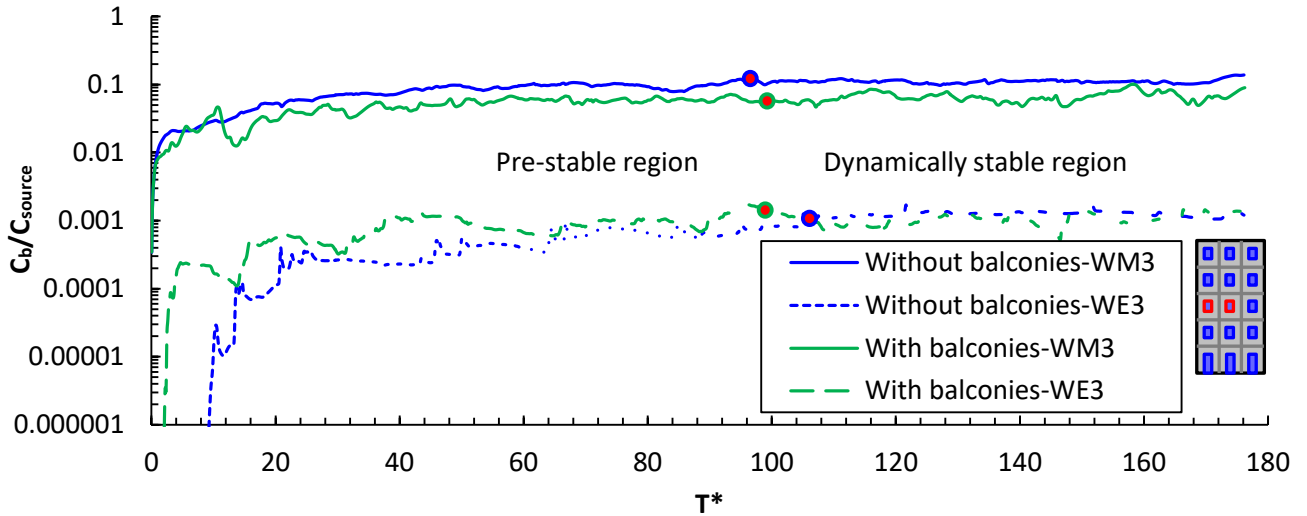
	Method	Physical model (X:Y:Z)	L_R/L L_W/L	
	Leitl and Schatzmann (1998)	Experiment	1:1.25:1.25	0.52 1.8
	Li and Meroney (1983)	Experiment	1:1:1	0.64 1.33
	Ai and Mak (2013b)	CFD-RANS	1:1.25:1.25	0.45 3.2
	Present simulation	CFD-LES	1:1.2:2.25	0.51 1.95

Table 2 compares the reattachment lengths on the roof and on downstream ground of bluff bodies under a normal wind condition. Comparison between the LES results with the two sets of experimental data generally justifies the present LES simulations of flow field around the

multistory buildings. The deviations between the LES predictions and the experiments could be attributed to two reasons: (a) the configurations of the physical models are different and (b) there are real units and openings in the present building models, whereas the experimental models are solid blocks.



(a) Evolution of ACH values over time



(b) Evolution of tracer gas concentrations over time and the times (marked with dots) commencing the dynamically stable region

Fig. 5 Time series of ACH values and tracer gas concentrations of some units in the multistory buildings under the normal incident wind.

Fig. 5 provides examples of the time series of ACH values and tracer gas concentrations of certain units in the multistory buildings. It can be seen from Fig. 5(a) that the ACH value of a

unit is always highly fluctuating. Detailed analyses of the fluctuating behaviors of a single-sided ventilation rate as well as the transient flow patterns around a single opening, under various wind directions, can be found in Ai and Mak (2014c). Owing to the highly fluctuating flow field, it is necessary to analyze the interunit dispersion transiently. As shown in Fig. 5(b), the continuous release of tracer gas in a source unit (namely, WM3) results in a quick elevation of the concentration level in that unit, and the accumulated tracer gas then starts to transmit to adjacent units (e.g., WEd3) at a later moment. Such interunit dispersion would eventually achieve a dynamically stable state. The times that separate the whole evolution period into the pre-stable period and the dynamically stable period are carefully identified through sensitivity tests. When a time is identified, the linear regression is made on a concentration curve within the dynamically stable period. A final time is selected if further changing this time result in no more than 5% of deviations to both the coefficient and the R^2 value of the regressed linear equation. For all wind directions, these final concentration levels in other units are, on average, two to four orders of magnitude lower than those in the corresponding source units.

Fig. 6 provides examples of the evolution of re-entry ratios over time after releasing tracer gas, where the maximum, mean, and standard deviation values of re-entry ratios within the dynamically stable periods are also calculated. Three observations can be made based on these time series of re-entry ratios. First, the re-entry ratio of a specific unit is always fluctuating, implying that using a mean re-entry ratio to describe an interunit dispersion is inaccurate. Second, the fluctuating intensities of re-entry ratios within the dynamically stable periods differ between different units, as indicated by the standard deviation values. The

re-entry characteristics during the dynamically stable periods are analyzed in Section 5. Third, there may be a large difference in the times when the re-entry ratios reach the mean value in different units. Such time scales of interunit dispersion are analyzed in Section 6.

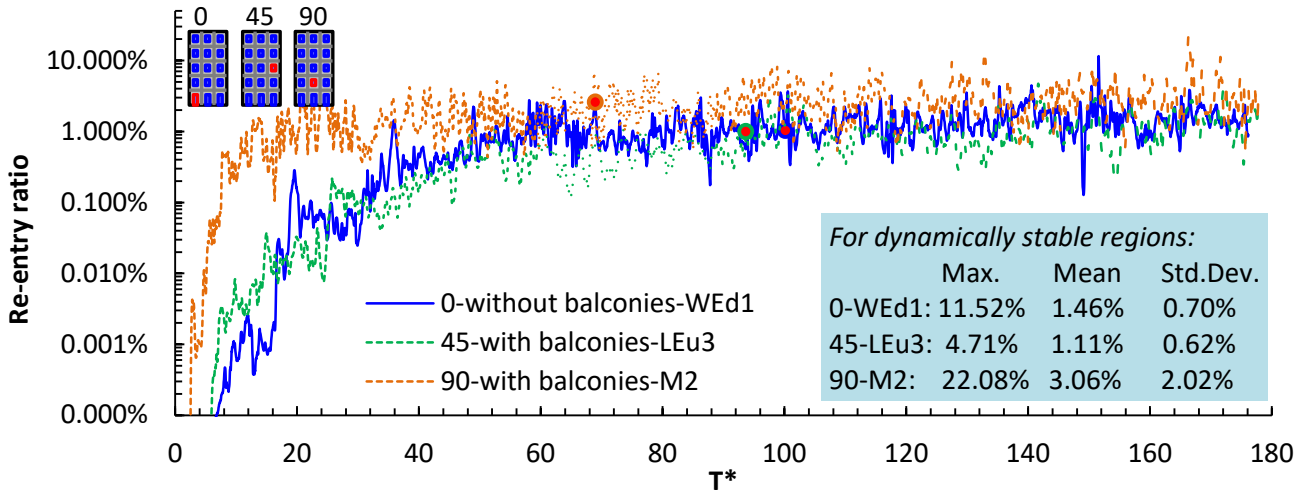
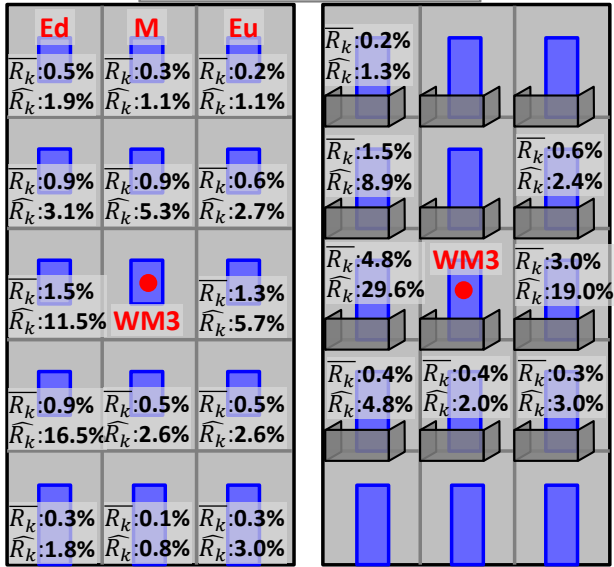
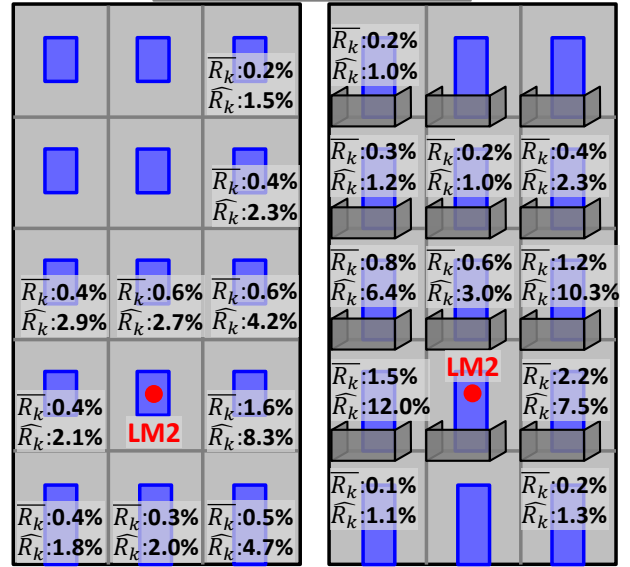
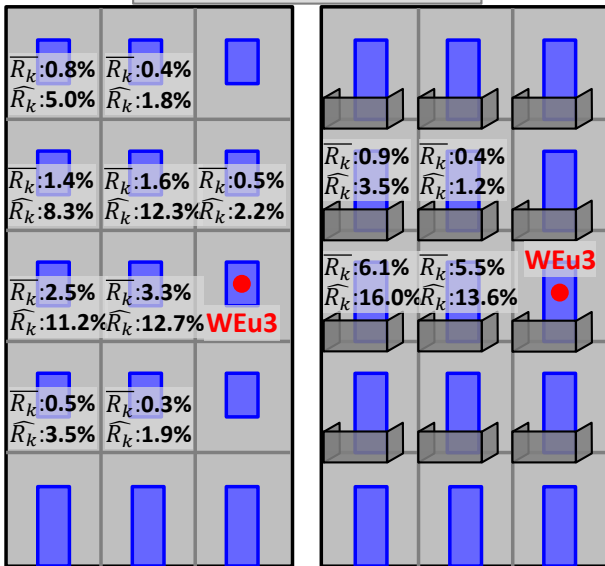
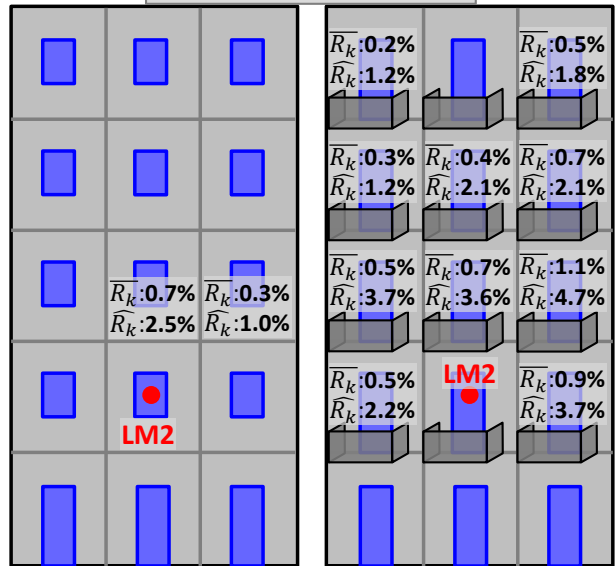


Fig. 6 Evolution of re-entry ratios over time and the maximum, mean, and standard deviation values within the dynamically stable periods; dots mark the times commencing the dynamically stable periods.

5. Results and analyses: Dispersion routes and re-entry ratios

This section analyzes the interunit dispersion characteristics during the dynamically stable periods. Fig. 7 presents the mean and maximum re-entry ratios of the tracer gas from source units to other units. The maximum values are provided, given that they are important to the infectious risk assessment. The threshold used to exclude results is re-entry ratio less than 0.1%.

(a) $\theta=0^\circ$ & windward side(b) $\theta=0^\circ$ & leeward side(c) $\theta=45^\circ$ & windward side(d) $\theta=45^\circ$ & leeward side

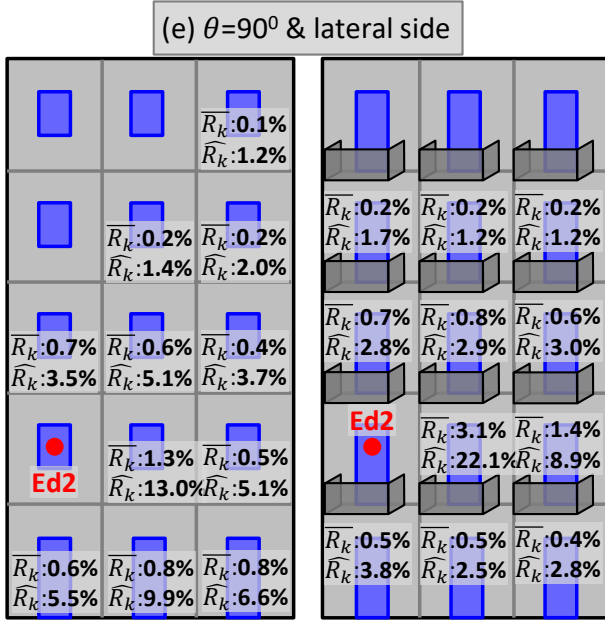


Fig. 7 Mean and maximum re-entry ratios of tracer gas from source units to other units during dynamically stable periods; \overline{R}_k represents mean re-entry ratio and \hat{R}_k maximum re-entry ratio.

Some previous studies also found that this stochastic feature of inflow does not necessarily result in statistical symmetry.

Fig. 7(a) presents the results on the windward side under a normal wind direction, when the tracer gas is released from unit WM3. The asymmetrical results occur between the two end units. Normally, velocity and pressure fields are easy to achieve aerodynamically symmetrical results, while the asymmetrical phenomenon likely appears on concentration field. Some previous wind tunnel experiments also found that asymmetrical concentration results exist between geometrically symmetrical observing locations (e.g., Liu et al., 2010). The possible reason for this difference is that the concentration transport is governed by more complex transport mechanisms than the velocity and pressure fields. Recently, it was found that there is an important concentration transport mechanism, namely the counter-gradient

mechanism (i.e., tracer gas transports from low-concentration areas to high-concentration areas), see for example Gousseau et al., 2011b. However, it is believed that further studies to explain the occurrence of the asymmetrical results are still necessary.

These results presented in Fig. (a) may lead to three conclusions. First, without balconies, the tracer gas disperses in all directions around the source unit, namely upward, downward, and lateral directions. This finding is inconsistent with previous RANS results (Ai et al., 2013a; Ai and Mak, 2014a), which show only downward dispersion. Such a difference between the findings of the RANS and LES simulations could be attributed to the inability of the RANS models to interpret the transiently fluctuating flows that deviate from the mean flow. Second, a unit with a very small mean re-entry ratio could occasionally experience very large re-entry ratios, such as unit WEd2 with $\overline{R_k}$ and $\overline{R_k}$ equal to 0.9% and 16.5%, respectively. This is an important finding, demonstrating that the mean RANS results are insufficient to describe real infectious risk circumstances. Third, the presence of balconies significantly aggravates the transmission to the two lateral units on the same floor of the source unit. Their presence shrinks the infectious scope, evidently because of their blockage and channel effects.

Fig. 7(b) presents the results on the leeward side under a normal wind direction, when the tracer gas is released from unit LM2. Similar to the windward side, the stochastic and fluctuating flows induce dispersion in all directions around the source unit. This, again, does not accord with previous RANS results, which suggest only upward dispersion. In particular, downward dispersion is found, which is produced by unsteady interaction between the large recirculation vortex behind the building and the small corner vortex at ground level (Ai and

Mak, 2014c). Unlike on the windward side, the presence of balconies broadens the infectious scope and elevates the re-entry ratios. This should be attributed to the fact that the negative wake region helps the leeward balconies accumulate and preserve the tracer gas.

Fig. 7(c) presents the results on the windward side under an oblique wind direction, when the tracer gas is released from unit WEu3. Without balconies, the tracer gas mainly disperses downstream, along which many units could be dangerous. This finding updates previous RANS simulations, which detected infections only in the two downstream units on the same floor as the source unit. Through the channel effect, the presence of balconies limits the dispersion to a smaller number of units, particularly to those on the same floor, which is very useful for the control of infection.

Fig. 7(d) presents the results on the leeward side under an oblique wind direction, when the tracer gas is released from unit LM2. Although the dispersion is only limited to the units on the floor above the source unit in the building without balconies, it is dangerous for almost all units in the building with balconies, except for those on the floor below the source unit. As under normal wind direction, the presence of balconies has the disadvantage of diluting the tracer gas. Such a large difference in dispersion characteristics between buildings with and without balconies (also other similar envelope features) should be given special attention in developing control measures.

Fig. 7(e) presents the results on a lateral side under a parallel wind direction, when the tracer gas is released from unit Ed2. The tracer gas released from the source unit disperses mainly in upward and upstream directions, though the downward dispersion is still significant. Units along these directions could suffer from re-entry and thus be dangerous. The presence

of balconies dramatically intensifies the dispersion in the downstream units, while it slightly mitigates the dispersion in other units. For both buildings, the infectious scopes predicted by LES simulations are much larger than those given by RANS simulations (Ai and Mak, 2014a).

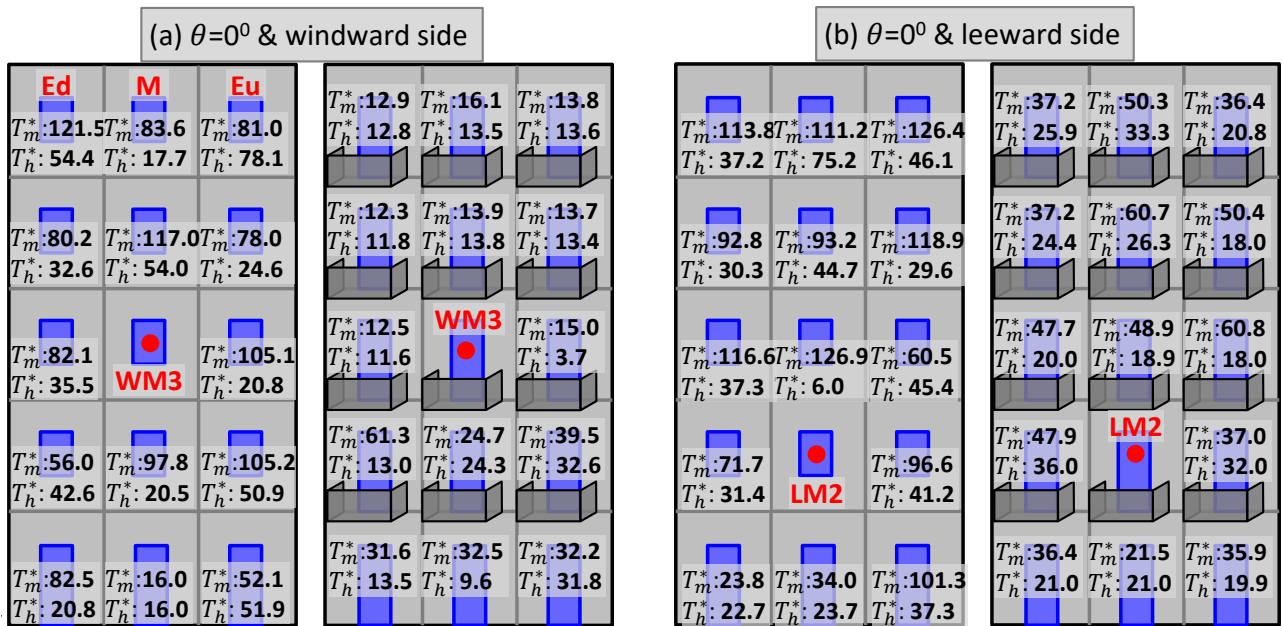
In addition to re-entry ratios, the standard deviations of re-entry ratios are also calculated to indicate their fluctuations (these figures are not presented). It is found that, for many units, the standard deviations are large enough to be comparable with the mean re-entry ratios. These levels of fluctuation in re-entry ratios should be considered when assessing infectious risk.

6. Results and analyses: Time scales of interunit dispersion

This section analyzes the time scales of interunit dispersion during the pre-stable periods. As re-entry ratio R_k is related to an ACH ratio, it could be very large even at the beginning of tracer gas release, see Fig. 6. Therefore, although R_k is useful to evaluate the dispersion characteristics during the dynamically stable periods, it is not sensitive to reveal time characteristics. This study uses the concentration ratio M_{i-j} between an infected unit and the source unit to examine the time scales of interunit dispersion.

Fig. 8 presents the nondimensional times required to reach both the mean and the half mean M_{i-j} values of the relevant units. The nondimensional times have the same definition with that specified in the caption of Fig.3. Fig. 8 shows two aspects worthy of discussion. The first is the influencing factors of the distribution and magnitude of the time scales. For a specific unit, the time scales do not show an obvious relation with its distance to the source unit and the approaching wind direction. However, the time scales on the buildings without

balconies scatter at a larger range than those with balconies. The relatively uniform distribution of time scales on the buildings with balconies should be ascribed to the fact that the balconies disturb the near-wall flow, resulting in a more dynamically stable envelope concentration field. Generally, under the normal and oblique wind directions, the time scales on windward sides are shorter than those on leeward sides, as larger pressure fields near the windward sides intensify quick dispersion of the tracer gas. The second aspect is the magnitudes of these time scales. The magnitudes of T_h^* values are mostly comparable with those of natural ventilation. Based on the present physical model, the nondimensional times required to achieve one whole-unit air replacement for the typical naturally ventilated ACH values of 5, 10, and 20 are 53.3, 26.7, and 13.3, respectively. Here these ACH values occur commonly in naturally ventilated buildings (Niu and Tung, 2008; Ai et al., 2013c). Such comparable magnitudes are to be expected as interunit dispersion occurs based on the natural ventilation system and the interunit dispersion is governed by the indoor and outdoor airflow exchange mechanisms.



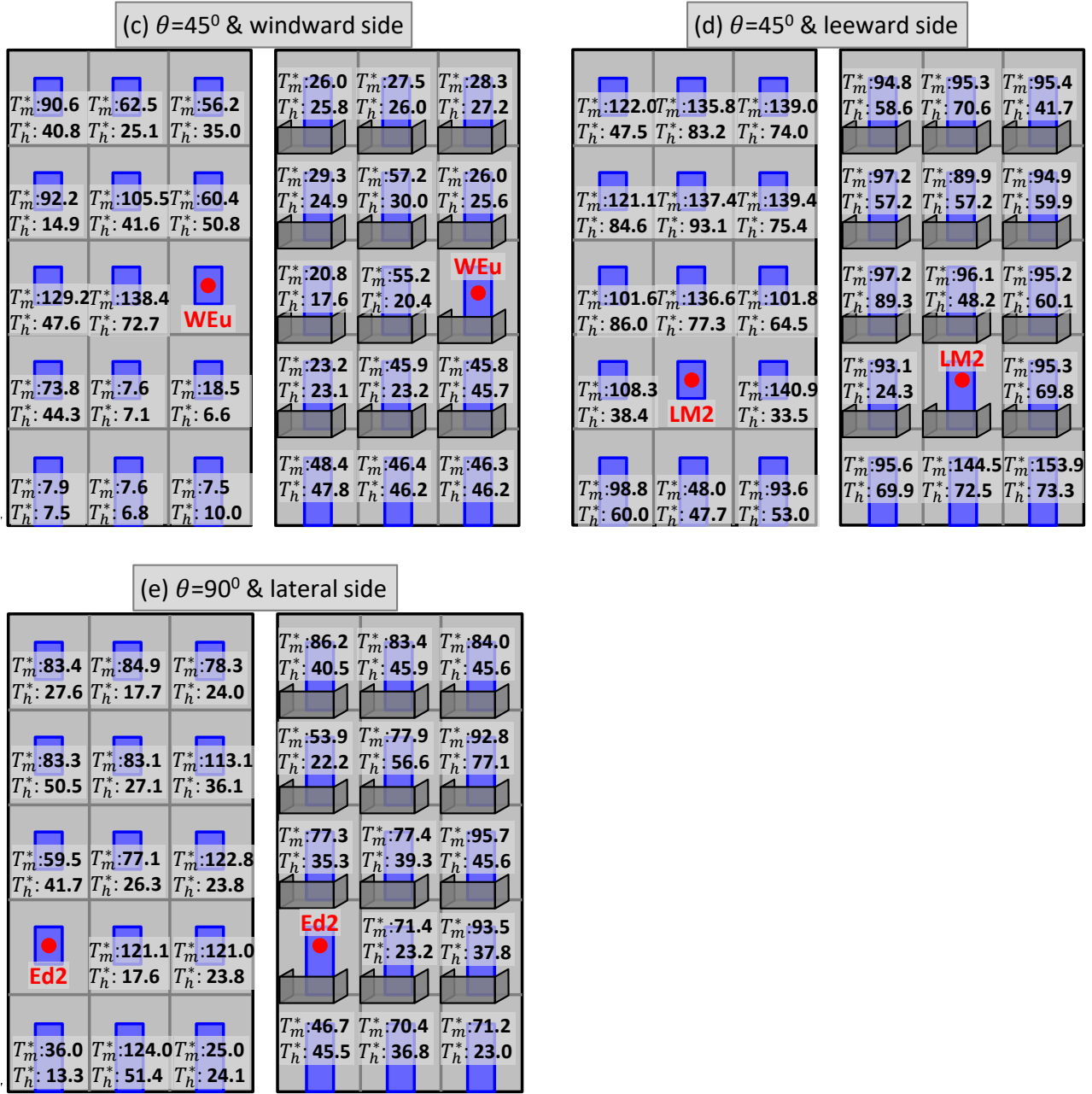


Fig. 8 Time scales of interunit dispersion from a source unit to its adjacent units; T_m^* and T_h^* represents the nondimensional times for reaching the mean and the half mean M_{i-j} values, respectively, where the mean M_{i-j} values are obtained by taking averages within the dynamically stable periods.

Table 3 A summary of the ranges of the times required to reach specific M_{i-j} values, where T_ϕ^* indicates the time required to reach the M_{i-j} value of ϕ ; NB indicates no balconies and

B balconies; NA indicates no unit reaching this level of M_{i-j} ; and those with only one number indicate only one unit reaching this level of M_{i-j} .

	$\theta = 0^\circ$ & windward side		$\theta = 0^\circ$ & leeward side		$\theta = 45^\circ$ & windward side		$\theta = 45^\circ$ & leeward side		$\theta = 90^\circ$ & lateral side	
	NB	B	NB	B	NB	B	NB	B	NB	B
$T_{0.0001}^*$	[4.4, 18.1]	[2.1, 31.8]	[3.2, 18.3]	[5.4, 19.6]	[6.4, 46.5]	[2.8, 48.2]	[13.2, 57.9]	[2.3, 69.6]	[9.7, 18.2]	[4.9, 17.4]
$T_{0.001}^*$	[13.5, 78.8]	[2.4, 32.6]	[4.8, 75.0]	[8.8, 35.7]	[7.2, 58.2]	[5.9, 59.6]	[26.6, 94.9]	[24.1, 84.4]	[9.9, 108.6]	[6.5, 103.5]
$T_{0.01}^*$	[82.5, 84.4]	[3.8, 12.6]	60.3	[32.1, 61.2]	[99.3, 174.4]	[14.4, 129.8]	NA	97.3	24.8	[16.7, 113.5]

Table 3 provides a summary of the time scales required to reach specific M_{i-j} values. From the viewpoint of the control of infection, there is a negligible difference in the time scales between different cases. Among these time scales, the ranges of $T_{0.0001}^*$ are particularly interesting, representing the times required to achieve M_{i-j} values of 1:10,000. Considering that a respiratory process, such as coughing and sneezing, can produce millions of aerosol particles (Duguid, 1946), $T_{0.0001}^*$ may represent the times required by the first stream of pathogen-laden aerosols to reach an infected unit. Previous particle simulations by Gao et al. (2009) suggested a comparable time scale to the first arrivals with the $T_{0.0001}^*$ values listed in Table 3. Generally, a shorter time is required to reach a specific M_{i-j} in a unit that is closer to the source unit (these figures are not presented).

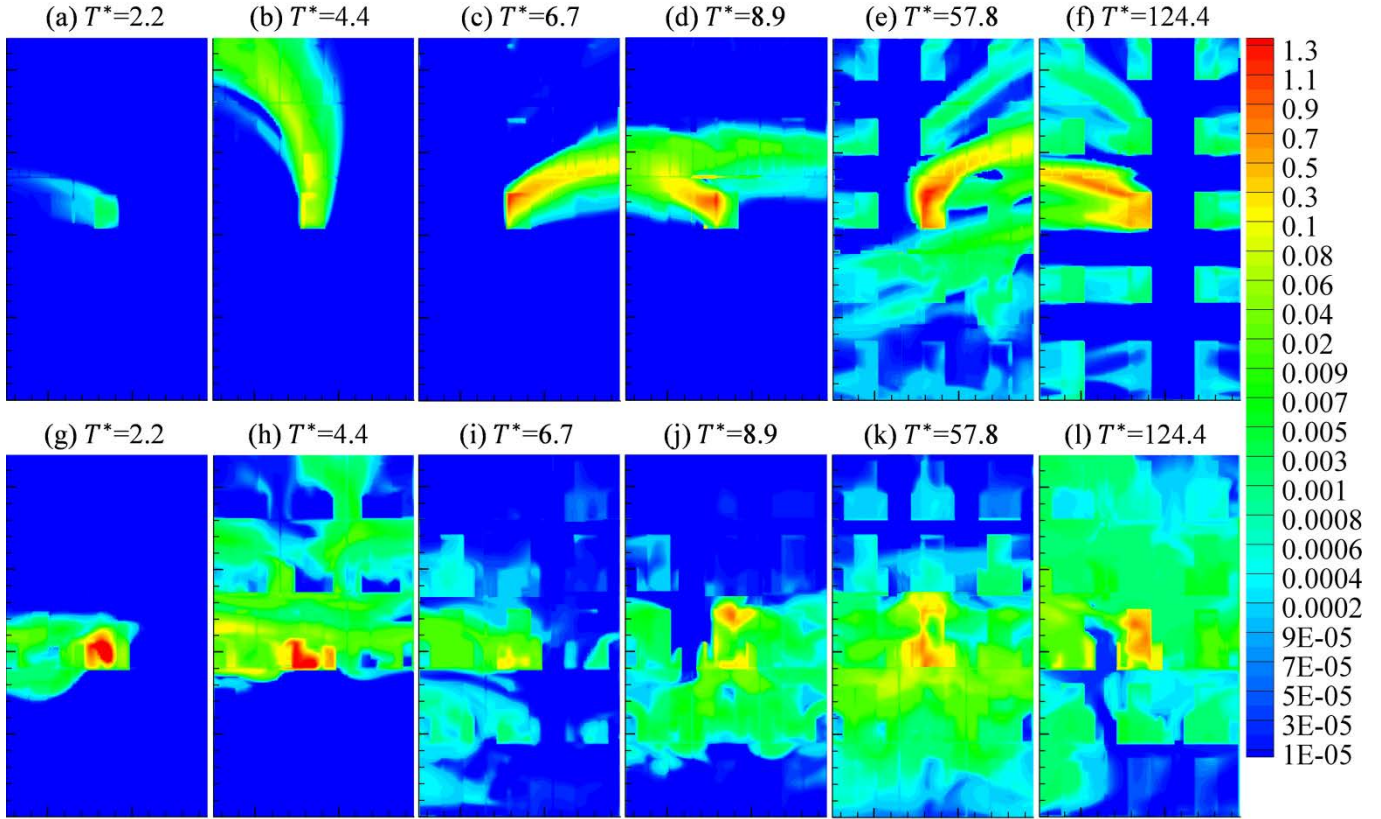


Fig. 9 Nondimensional concentration distributions on the windward facades of buildings under normal wind direction at various moments; (a)-(f) present the building without balconies and (g)-(l) present the building with balconies.

In order to further examine the time characteristics of interunit dispersion, we analyze the concentration distributions on building facades at various moments. Fig. 9 presents the nondimensional concentration (nondimensionalized by C_i) distributions on the windward facades of the buildings under normal wind direction at six different moments. Based on Fig. 9, three observations can be made. First, dispersion route is not constant, the main dispersion direction varies with time. This variation is stochastic, implying that the incursion of pollutants into a specific unit is intermittent. Such characteristics significantly broaden the dispersion scope and thus increase the difficulty of control. Second, there could be secondary interunit dispersions around multistory buildings, as shown clearly in Fig. 9 (e) and (f).

Secondary dispersion could be an important mechanism of interunit dispersion. It indicates that a portion of pollutants entering a specific unit could come from an infected unit, rather than directly from the source unit. This feature also contributes to extending dispersion scope and increases dispersion uncertainty. Third, the presence of balconies helps increase the uniformity of pollutant distribution on the buildings' facades, as their presence hinders the development of main dispersion directions. These envelope dispersion characteristics under normal wind direction represent the general dispersion circumstances of other cases not presented in this paper.

7. Further discussion

The results and analyses presented in the previous sections provide an overview of the characteristics of transient interunit dispersion around multistory buildings. This section presents further discussion of the infectious risk of this dispersion more broadly within the field of epidemiology and building ventilation.

According to the well-known Wells-Riley model (Riley et al., 1978), the number of infectious quanta produced by infector(s) and the duration of exposure time are two key factors influencing the infectious risk of a susceptible person. Within a specific unit, the number of infectious quanta may be estimated by the re-entry quantity of infected air originating from the source unit, based on the concentration of pathogens. Such re-entry quantities in various circumstances are provided in the present study. However, the present study cannot provide a universal safe threshold for the re-entry ratio to estimate the infectious risk for a specific unit, as the size of a quantum is strongly related to the type of pathogen and the physical condition of susceptible persons. Previous studies by Franz et al. (1997) showed

that many pathogens can cause disease with several to dozens of organisms, such as viral hemorrhagic fevers (1-10), Q fever (1-10), tularemia (10-50), brucellosis (10-100), and smallpox (10-100). For highly infectious bacteria like *M. tuberculosis*, even a single organism is sufficient to cause disease, while a cough may produce around 3,000 organisms (Duguid, 1946; Fitzgerald and Haas, 2005). When exposed to a certain concentration level of a pathogen, the exposure time should be controlled. Isolating the infectors as early as possible to reduce exposure time and ventilating the suspected regions sufficiently are effective methods (Tang et al., 2006) to control infection.

Another aspect that is important to the estimation of airborne infectious risk is the ratio of two time scales: the time scale required to accumulate a quantum and the time scale of the pathogen's survival. To the best of the authors' knowledge, the two time scales have not been compared previously. The prerequisite of the occurrence of an airborne infection is that at least a quantum of organisms produced by an infector must remain both airborne and survive to be inhaled by a susceptible person (Tang et al., 2006). If the pathogen's survival time is shorter than the time scale needed to accumulate a quantum of this pathogen in a target unit, the occupants in this unit are safe and thus no protective measures are required. Unfortunately, previous data have shown that many pathogens can survive in aerosols for a very long time, such as human coronavirus 229E, which survives for several to dozens of hours (Ijaz et al., 1985); influenza viruses, which survives for up to 24 hours (Loosli et al., 1943); and SARS coronavirus, which survives for more than seven days (Lai et al., 2005). These survival times are much longer than the time scales of interunit dispersion. However, the survival time of a pathogen is affected by many factors (Morawska, 2006; Tang et al., 2006). In certain

circumstances, the survival time of a SARS virus is only several minutes (WHO, 2003), a period comparable with most interunit dispersion time scales. Therefore, for a specific pathogen under a certain physical environment, it is meaningful and necessary to make a comparison of its survival time and the time scales of interunit dispersion in order to take more accurate and effective intervention measures.

8. Summary and conclusions

This paper has investigated wind-induced interunit dispersion around multistory buildings using the LES model. The reliability of the LES model was assured with experimental validation and sensitivity tests. This study proposes a method that avoids the occurrence of solution oscillation after the introduction of the concentration equation.

Continuous release of tracer gas in a source unit results in a quick elevation of concentration level in this unit, and the accumulated tracer gas starts to transmit to adjacent units at a later moment. Such an interunit dispersion would eventually achieve a dynamically stable state, with re-entry ratios always fluctuating around their mean values. The main dispersion routes always vary with time, implying that the incursion of pollutants into a specific unit is intermittent. In addition, secondary dispersions are observed. These two dispersion route features contribute to extended dispersion scope and increased dispersion uncertainty.

In order to facilitate analyses, the transient interunit dispersion processes were divided into two periods, namely pre-stable and dynamically stable periods. For the pre-stable periods, the nondimensional times required to reach the mean and half mean M_{i-j} values were analyzed. These time scales of a unit are influenced negligibly by distance from the source unit and the

approaching wind direction, which, generally, are shorter on the windward sides than the leeward sides. The magnitudes of the time scales of reaching the half mean M_{i-j} values are mostly comparable with those of natural ventilation.

For dynamically stable periods, the mean and maximum re-entry ratios as well as their standard deviations were analyzed. LES simulations reveal much larger infectious scopes than previous RANS simulations. A unit with a very small mean re-entry ratio could occasionally experience very large re-entry ratios. For many units, the standard deviations of re-entry ratios are large enough to be comparable with the mean re-entry ratios. These findings demonstrate that the previous RANS results are insufficient to describe the actual infectious risk circumstances. In addition, the presence of balconies helps shrink and broaden the infectious scope on the windward and leeward sides, respectively, which also helps create more stable and uniform envelope concentration fields.

The general re-entry ratios and dispersion time scales provided by the present study are useful for infectious risk assessment and the development of control measures, based on the infectious and survival characteristics of a certain type of pathogen.

Acknowledgements

The authors would like to thank sincerely the anonymous reviewers for their very constructive comments and suggestions, which have substantially improved the quality of this paper.

References

- Ai, Z.T. and Mak, C.M. (2013b) CFD simulation of flow and dispersion around an isolated building: Effect of inhomogeneous ABL and near-wall treatment, *Atmos. Environ.*, **77**, 568-578.
- Ai, Z.T. and Mak, C.M. (2014a) A study of interunit dispersion around multistory buildings

- with single-sided ventilation under different wind directions, *Atmos. Environ.*, **88**, 1-13.
- Ai, Z.T. and Mak, C.M. (2014b) Modeling of coupled urban wind flow and indoor air flow on a high-density near-wall mesh: Sensitivity analyses and case study for single-sided ventilation, *Environ. Modell. Softw.*, **60**, 57-68.
- Ai, Z.T. and Mak, C.M. (2014c) Analysis of fluctuating characteristics of wind-induced airflow through a single opening using LES modeling and the tracer gas technique, *Build. Environ.*, **80**, 249-258.
- Ai, Z.T. and Mak, C.M. (2014d) Large-eddy simulation of flow and dispersion around an isolated building: Analysis of influencing factors, *Comput. Fluids*, under review.
- Ai, Z.T., Mak, C.M. and Cui, D.J. (2013c) On-site measurements of ventilation performance and indoor air quality in naturally ventilated high-rise residential buildings in Hong Kong, *Indoor Built Environ.*, In press, Doi: 10.1177/1420326X13508566.
- Ai, Z.T., Mak, C.M. and Niu, J.L. (2013a) Numerical investigation of wind-induced airflow and interunit dispersion characteristics in multistory residential buildings, *Indoor Air*, **23**, 417-429.
- Barker, J., Stevens, D. and Bloomfield, S.F. (2001) Spread and prevention of some common viral infections in community facilities and domestic homes, *J. Appl. Microbiol.*, **91**, 7-21.
- Brundrett, G.W. (1992) *Legionella and building services*, Oxford, Butterworth-Heinemann.
- Building Department, Lands Department and Planning Department, Hong Kong (2001) Joint Practice Note No. 1: Green and innovative buildings. Hong Kong Special Administrative Region.
- Caciolo, M., Stabat, P. and Marchio, D. (2012) Numerical simulation of single-sided ventilation using RANS and LES and comparison with full-scale experiments, *Build. Environ.*, **50**, 202-213.
- Centers for Disease Control and Prevention (CDCP) (1994) Guidelines for preventing the transmission of *Mycobacterium tuberculosis* in health-care facilities, *MMWR Recomm. Rep.*, **43**, 1-132.
- Cole, E.C. and Cook, C.E. (1998) Characterization of infectious bio-aerosols in health care facilities: An aid to effective engineering controls and preventive strategies, *Amer. J. Infection Control*, **26**, 453-464.
- Dascalaki, E., Santamouris, M., Argiriou, A., Helmis, C., Asimakopoulos, D.N., Papadopoulos, K. and Soilemes, A. (1996) On the combination of air velocity and flow measurements in single sided natural ventilation configurations, *Energy Buildings*, **24**, 155-165.
- Duguid, J.P. (1946) The size and duration of air-carriage of respiratory droplets and droplet-nuclei, *J. Hyg.*, **4**, 471-480.

- Etheridge, D. (2011) Natural ventilation of buildings: Theory, measurement and design, Wiley, UK.
- Fitzgerald, D. and Haas, D.W. (2005) Mycobacterium tuberculosis. In: Mandell, G.L., Bennett, J.E., Dolin, R., eds., Principles and practice of infectious diseases, 6th ed., Philadelphia: Churchill Livingstone, pp. 2852-2886.
- Fluent (2010) ANSYS FLUENT 13.0 Theory Guide, Turbulence, ANSYS Inc., Canonsburg, PA.
- Franke, J., Hellsten, A., Schlünzen, H. and Carissimo, B. (2007) Best practice guideline for the CFD simulation of flows in the urban environment, COST Office, Brussels, ISBN 3-00-018312-4.
- Franz, D.R., Jahrling, P.D., Friedlander, A.M., McClain, D.J., Hoover, D.L., Bryne, W.R., Pavlin, J.A., Christopher, G.W. and Eitzen, E.M. Jr. (1997) Clinical recognition and management of patients exposed to biological warfare agents, *J. Am. Med. Assoc.*, **278**(5), 399-411.
- Gao, N.P. and Niu, J.L. (2007) Modeling particle dispersion and deposition in indoor environments, *Atmos. Environ.*, **41**, 3862-3876.
- Gao, N.P., Niu, J.L., Perino, M. and Heiselberg, P. (2008) The airborne transmission of infection between flats in high-rise residential buildings: Tracer gas simulation, *Build. Environ.*, **43**, 1805-1817.
- Gao, N.P., Niu, J.L., Perino, M. and Heiselberg, P. (2009) The airborne transmission of infection between flats in high-rise residential buildings: Particle simulation, *Build. Environ.*, **44**, 402-410.
- Gousseau, P., Blocken, B., Stathopoulos, T. and van Heijst, G.J.F. (2011a) CFD simulation of near-field pollutant dispersion on a high-resolution grid: A case study by LES and RANS for a building group in downtown Montreal, *Atmos. Environ.*, **45**, 428-438.
- Gousseau, P., Blocken, B., and van Heijst, G.J.F. (2011b) CFD simulation of pollutant dispersion around isolated buildings: On the role of convective and turbulent mass fluxes in the prediction accuracy, *J. Hazard. Mater.*, **194**, 422-434.
- Haghighat, F., Brohus, H. and Rao, J. (2000) Modeling air infiltration due to wind fluctuations – a review, *Build. Environ.*, **35**, 377-385.
- Haghighat, F., Rao, J. and Fazio, P. (1991) The influence of turbulent wind on air change rates – a modeling approach, *Build. Environ.*, **26**(2), 95-109.
- Health, Welfare & Food Bureau, Government of the Hong Kong Special Administrative Region (HWFB-HK) (2003) SARS Bulletin (28 May 2003). Available at: <http://www.info.gov.hk/info/sars/bulletin/bulletin0528e.pdf>, accessed 20 September, 2012.
- Hinze, J.O. (1975) Turbulence, McGraw-Hill Publishing CO., New York.

- Hodgson, M.J., Miller, S.L., Li, Y., McCoy, W.F., Parsons, S.A., Schoen, L.J. and Sekhar, C. (2012) Airborne Infectious Diseases, ASHRAE Position Document, Atlanta, Georgia.
- Iizuka, S. and Kondo, H. (2004) Performance of various sub-grid scale models in large-eddy simulations of turbulent flow over complex terrain, *Atmos. Environ.*, **38**, 7083-7091.
- Ijaz, M.K., Brunner, A.H., Sattar, S.A., Nair, R.C. and Johnson-Lussenburg, C.M. (1985) Survival characteristics of airborne human coronavirus 229E, *J. Gen. Virol.*, **66**, 2743-2748.
- Jiang, Y. and Chen, Q. (2001) Study of natural ventilation in buildings by large eddy simulation, *J. Wind Eng. Ind. Aerodyn.*, **89**, 1155-1178.
- Lai, M.Y., Cheng, P.K. and Lim, W.W. (2005) Survival of severe acute respiratory syndrome coronavirus, *Clin. Infect. Dis.*, **41**, e67-e71.
- Leitl, B. and Schatzmann, M. (1998) CEDVAL at Hamburg University, <http://www.mi.uni-hamburg.de/Data-Sets.432.0.html>, accessed 20 May 2013.
- Li, W.W. and Meroney, R.N. (1983) Gas dispersion near a cubical model building, Part 1, mean concentration measurements, *J. Wind Eng. Ind. Aerodyn.*, **12**, 15-33.
- Li, Y., Duan, S., Yu, I.T.S. and Wong, T.W. (2005a) Multi-zone modeling of probable SARS virus transmission by airflow between flats in Block E, Amoy Gardens, *Indoor Air*, **15**, 95-111.
- Li, Y., Huang, X., Yu, I.T.S., Wong, T.W. and Qian, H. (2005b) Role of air distribution in SARS transmission during the largest nosocomial outbreak in Hong Kong, *Indoor Air*, **15**, 83-95.
- Lilly, D.K. (1992) A proposed modification of the Germano subgrid-scale closure method, *Phys. Fluids A*, **4**, 633-635.
- Linden, P.F. (1999) The fluid mechanics of natural ventilation, *Annu. Rev. Fluid Mech.*, **31**, 201-238.
- Liu, X.P., Niu, J.L. and Kwok, K.C.S. (2011a) Analysis of concentration fluctuations in gas dispersion around high-rise building for different incident wind directions, *J. Hazard. Mater.*, **192**, 1623-1632.
- Liu, X.P., Niu, J.L., Kwok, K.C.S., Wang, J.H. and Li, B.Z. (2010) Investigation of indoor air pollutant dispersion and cross-contamination around a typical high-rise residential building: Wind tunnel tests, *Build. Environ.*, **45**, 1769-1778.
- Liu, X.P., Niu, J.L., Kwok, K.C.S., Wang, J.H. and Li, B.Z. (2011b) Local characteristics of cross-unit contamination around high-rise building due to wind effect: Mean concentration and infection risk assessment, *J. Hazard. Mater.*, **192**, 160-167.
- Loosli, C., Lemon, H., Robertson, O. and Appel, E. (1943) Experimental airborne influenza infection: 1. Influence of humidity on survival of virus in air, *Proc. Soc. Exp. Biol. Med.*,

53, 205-206.

- Mathey, F., Cokljat, D., Bertoglio, J.P. and Sergent, E. (2006) Assessment of the vortex method for large eddy simulation inlet conditions, *Progr. Comput. Fluid Dynam.*, **6**, 58-67.
- Mendell, M.J., Fisk, W.J., Kreiss, K., Levin, H., Alexander, D., Cain, W.S., Girman, J.R., Hines, C.J., Jensen, P.A., Milton, D.K., Rexroat, L.P. and Wallingford, K.M. (2002) Improving the health of workers in indoor environments: priority research needs for a national occupational research agenda, *Amer. J. Public. Health*, **92**, 1430-1440.
- Mfula, A.M., Kukadia, V., Griffiths, R.F. and Hall, D.J. (2005) Wind tunnel modeling of urban building exposure to outdoor pollution, *Atmos. Environ.*, **39**, 2737-2745.
- Mitman, M. (1945) Aerial infection, *Brit. Med. J.*, **1**, 71-74.
- Morawska, L. (2006) Droplet fate in indoor environments, or can we prevent the spread of infection? *Indoor Air*, **16**, 335-347.
- Morawska, L., Afshari, A., Bae, G.N., Buonanno, G., Chao, C.Y.H, Hänninen, O., Hofmann, W., Isaxon, C., Jayaratne, E.R., Pasanen, P., Salthammer, T., Waring, M. and Wierzbicka, A. (2013) Indoor aerosols: From personal exposure to risk assessment, *Indoor Air*, **23**, 462-487.
- Murakami, S. (1993) Comparison of various turbulence models applied to a bluff body, *J. Wind Eng. Ind. Aerodyn.*, **46 & 47**, 21-36.
- Nicas, M., Nazaroff, W.W. and Hubbard, A. (2005) Toward understanding the risk of secondary airborne infection: Emission of respirable pathogens, *J. Occup. Environ. Hyg.*, **2**, 143-154.
- Niu, J.L. and Tung, T.C.W. (2008) On-site quantification of re-entry ratio of ventilation exhausts in multi-family residential buildings and implications, *Indoor Air*, **18**, 12-26.
- Richardson, L.F. (1910) The approximate arithmetical solution by finite differences of physical problems involving differential equations, with an application to the stresses in a masonry dam, *Philos. Trans. R. Soc. Lond.*, **210**, 307-357.
- Riley, E.C., Murphy, G. and Riley, R.L. (1978) Airborne spread of measles in a suburban elementary school, *Am. J. Epidemiol.*, **107**, 421-432.
- Roache, P.J. (1994) Perspective: A method for uniform reporting of grid refinement studies, *ASME J. Fluids Eng.*, **116**, 405-413.
- Rodi, W. (1997) Comparison of LES and RANS calculations of the flow around bluff bodies, *J. Wind Eng. Ind. Aerodyn.*, **69-71**, 55-75.
- Salim, S.M., Buccolieri, R., Chan, A. and Sabatino, S.D. (2011) Numerical simulation of atmospheric pollutant dispersion in an urban street canyon: Comparison between RANS and LES, *J. Wind Eng. Ind. Aerodyn.*, **99**, 103-113.
- Smagorinsky, J. (1963) General circulation experiments with the primitive equations: The

- basic experiment, *Mon. Weather Rev.*, **91**, 99-164.
- Straw, M.P. (2000) Computation and measurement of wind induced ventilation, thesis, University of Nottingham.
- Tabor, G.R. and Baba-Ahmadi, M.H. (2010) Inlet conditions for large eddy simulation: A review, *Comput. Fluids*, **39**, 553-567.
- Tang, J.W., Li, Y., Eames, I., Chan, P.K.S. and Ridgway, G.L. (2006) Factors involved in the aerosol transmission of infection and control of ventilation in healthcare premises, *J. Hosp. Infect.*, **64**, 100-114.
- Tellier, R. (2006) Review of aerosol transmission of influenza A virus, *Emerg. Infect. Diseases*, **12**, 1657-1662.
- Thomas, R.J. (2013) Particle size and pathogenicity in the respiratory tract, *Virulence*, **4**(8), 847-858.
- Tominaga, Y., Mochida, A., Yoshie, R., Kataoka, H., Nozu, T., Yoshikawa, M. and Shirasawa, T. (2008) AIJ guidelines for practical applications of CFD to pedestrian wind environment around buildings, *J. Wind Eng. Ind. Aerodyn.*, **96**(10, 11), 1749-1761.
- Tominaga, Y. and Stathopoulos, T. (2010) Numerical simulation of dispersion around an isolated cubic building: Model evaluation of RANS and LES, *Build. Environ.*, **45**, 2231-2239.
- Tominaga, Y. and Stathopoulos, T. (2011) CFD modeling of pollution dispersion in a street canyon: Comparison between LES and RANS., *J. Wind Eng. Ind. Aerodyn.*, **99**, 340-348.
- van Hooff, T. and Blocken, B. (2010) Coupled urban wind flow and indoor natural ventilation modelling on a high-resolution grid: A case study for the Amsterdam ArenA stadium. *Environ. Modell. Softw.*, **25**, 51-65.
- Wang, J.H., Niu, J.L., Liu, X.P. and Yu, C.W.F. (2010) Assessment of pollutant dispersion in the re-entrance space of a high-rise residential building, using wind tunnel simulations, *Indoor Built Environ.*, **19**, 638-647.
- Wells, W.F. (1934) On air-borne infection, Study II, Droplets and droplet nuclei, *Am. J. Hyg.*, **20**, 611-618.
- World Health Organization (WHO) (2003) First data on stability and resistance of SARS coronavirus compiled by members of the WHO Laboratory Network. Available at: http://www.who.int/csr/sars/survival_2003_05_04/en/, accessed 14 August, 2014.
- Xie, X., Li, Y., Chwang, A.T.Y., Ho, P.L. and Seto, W.H. (2007) How far droplets can move in indoor environments – revisiting the wells evaporation-falling curve, *Indoor Air*, **17**, 211-225.
- Yoshie, R., Mochida, A., Tominaga, Y., Kataoka, H., Harimoto, K., Nozu, T. and Shirasawa, T. (2007) Cooperative project for CFD prediction of pedestrian wind environment in the

Architectural Institute of Japan, *J. Wind Eng. Ind. Aerodyn.*, **95(9, 11)**, 1551-1578.

Yu, I.T., Li, Y., Wong, T.W., Tam, W., Chan, A.T., Lee, J.H., Leung, D.Y. and Ho, T. (2004)
Evidence of airborne transmission of the severe acute respiratory syndrome virus, *N. Engl. J. Med.*, **350**, 1731-1739.